Proceedings of 2004 IEEE/RSJ International Conference on
Intelligent Robots and Systems
September 28 - October 2, 2004, Sendai, Japan

External Impulse of Single and Dual-Arm Sawing Tasks via Concept of Effective Mass; Modeling and Experiments

Jae Hoon Lee, Byung-Ju Yi and Il Hong Suh
School of Electrical Engineering and Computer Science
Hanyang University
Ansan, Korea
bj@hanyang.ac.kr

Sang-Rok Oh
Intelligent Robotics Research Center
KIST
Seoul, Korea
sroh@kist.re.kr

***Abstract*—Some of manufacturing tasks such as sawing task often require continuous impulsive motion. In case of sawing task, such impulsive motions can be observed between the teeth of the saw and the object being sawn. The amount of the external impulse exerted on the object is treated as an important control parameter in the sawing task.**

The purpose of this work is to show the efficacy of sawing task by using a dual-arm. For this, a new concept of effective mass is introduced to model the impact phenomenon in the sawing task. Using this concept, the external impulse model of sawing tasks is suggested. The optimal sawing region is identified in which the amount of external impulse is maximized. It is demonstrated through simulation and experiment that the dual-arm exhibits better sawing performance over a single arm in aspects of external impulse.

Keywords-Impulse; Dual Arm; Sawing; Effective Mass

I. INTRODUCTION

It is believed that robot manipulators will be appropriate for the light machining tasks. However, for the effective operation in such tasks, we have to take into account the physical characteristics of such tasks. For example, in sawing task, continuous impulsive motion is required between the teeth of the saw and the object being sawn. Another important feature of manufacturing tasks is the plastic deformation of the object. The sawn parts are deformed permanently by the sawing.

Figure 1. Human Sawing Task

Fig. 1 shows the human sawing task. The external impulse acting on the object in manufacturing tasks is the function of the posture and the dynamic characteristic of the worker. In most of robot control problems dealing with impact, the robot is controlled to minimize the amount of external impulse transmitted to the robot upon abrupt contact. On the contrary, the amount of external impulse should be maximized in some manufacturing tasks. However, the internal impulse experienced at the joints of the human-body should be minimized to avoid injury or damage. For such purpose, human usually identifies how to saw and where to saw by experiences. But, the robot should be trained to perform the sawing task effectively.

Methods to evaluate impulses occurring in general collisions have been proposed by several researchers [1-4, 6-9]. Walker investigated the external impulse model for serial-type manipulators and also proposed an impact measure for kinematically redundant and multiple armed robotic systems [1]. Liao and Leu [2] presented the Lagrangian external impact model to derive an impact equation for an industrial manipulator. Zheng and Hemami [3] derived the internal impulse model at the joints by using Newton-Euler equations, but their model was confined to serial-type manipulators. Wittenburg[4] provided a general methodology, in an implicit form, for modeling external and internal impulses. However, this model is not directly applicable to robotic systems. Kim, et al. [6] proposed a normalized impact geometry and performance measure based on velocity direction. However, their algorithm was confined to external impulse model for serial robotic system. Lee and Yi, et al. [7] proposed a closed-form, explicit external and internal impulse models for general classes of multi-body mechanisms. And, Lee and Yi, et al. [9] suggested an external impulse model and an internal impulse measure for sawing task to show the efficiency of sawing task by using a dual-arm. However, the previous algorithm was solely based on simulation results without any experimental verification.

Multiple cooperating robots can perform tasks more efficiently, which cannot be carried out by using a single arm. These tasks include the handling of heavy and large objects, and assembly of complex parts or part mating, and so on. One of the typical features of such multiple robot systems is redundant actuation mode. This mode enhances the performances of the system in aspects of singularity avoidance, increase of payload, stiffness, and development of multiple sub-criteria.

In this work, we investigate the advantage of dual-arm or multiple arms in the viewpoint of impulses. This paper deals with a new concept of an effective mass in sawing task and suggests an external impulse model for sawing task. It is demonstrated through simulation and experiment that the proposed external impulse model is coincident to the experimental result.

II. EXTERNAL IMPULSE MODEL FOR SAWING TASK

Most generally, the impact is partially elastic in the range of $0 < e < 1$. When the coefficient of restitution e is known, the relative velocity of colliding bodies can be obtained immediately after the impact. The component of the increment of relative velocity along a vector $\boldsymbol{n}$ that is normal to the contact surface is given by [4]

$$(\Delta \boldsymbol{v}_1 - \Delta \boldsymbol{v}_2)^T \boldsymbol{n} = -(1+e)(\boldsymbol{v}_1 - \boldsymbol{v}_2)^T \boldsymbol{n}, \qquad (1)$$

where $\boldsymbol{\upsilon}_1$ and $\boldsymbol{\upsilon}_2$ are the absolute velocities of the colliding bodies immediately before impact, and $\Delta\boldsymbol{\upsilon}_1$ and $\Delta\boldsymbol{\upsilon}_2$ are the velocity increments immediately after impact.

When a robot system interacts with environment, the dynamic model of the robot referenced to the independent joint set is given by

$$\boldsymbol{T}_a = [\boldsymbol{I}^*_{aa}]\ddot{\boldsymbol{\phi}}_a + \dot{\boldsymbol{\phi}}_a^T[\boldsymbol{P}^*_{aaa}]\dot{\boldsymbol{\phi}}_a - [\boldsymbol{G}_a^{\upsilon_I}]^T\boldsymbol{F}_I, \quad (2)$$

where $\boldsymbol{T}_a$ denotes the inertial load vector referenced to the independent joint set. $[\boldsymbol{I}^*_{aa}]$ and $[\boldsymbol{P}^*_{aaa}]$ represent the inertia matrix and the inertia power array referenced to the independent joint set, respectively[7]. And $\boldsymbol{F}_I$ is the impulsive external force at the contact point and $[\boldsymbol{G}_a^{\upsilon_I}] \in \Re^{3\times N_a}$ is the 1st order KIC relating the contact point velocity $\boldsymbol{\upsilon}_I$ with respect to the inertial frame to the independent joint velocity.

$$\boldsymbol{\upsilon}_I = [\boldsymbol{G}_a^{\upsilon_I}]\dot{\boldsymbol{\phi}}_a. \quad (3)$$

Integration of the dynamic model given in Eq. (2) over contacting time interval gives

$$\int_{t_0}^{t_0+\Delta t}\boldsymbol{T}_a dt = \int_{t_0}^{t_0+\Delta t}[\boldsymbol{I}^*_{aa}]\ddot{\boldsymbol{\phi}}_a dt + \int_{t_0}^{t_0+\Delta t}\dot{\boldsymbol{\phi}}_a^T[\boldsymbol{P}^*_{aaa}]\dot{\boldsymbol{\phi}}_a dt - \int_{t_0}^{t_0+\Delta t}[\boldsymbol{G}_a^{\upsilon_I}]^T\boldsymbol{F}_I dt. \quad (4)$$

Since the positions and velocities are finite at all times as $\Delta\boldsymbol{t}$ goes to zero, the integral term involving $\dot{\boldsymbol{\phi}}_a^T[\boldsymbol{P}^*_{aaa}]\dot{\boldsymbol{\phi}}_a$ becomes zero, as does that involving actuation input $\boldsymbol{T}_a$. Thus, we obtain the following simple expression[1]

$$[\boldsymbol{I}^*_{aa}]\left(\dot{\phi}(\boldsymbol{t}_0+\Delta\boldsymbol{t}) - \dot{\phi}(\boldsymbol{t}_0)\right) = [\boldsymbol{G}_a^{\upsilon_I}]^T\tilde{\boldsymbol{F}}_I, \quad (5)$$

where $\hat{\boldsymbol{F}}_I = \int_{t_0}^{t_0+\Delta t}\boldsymbol{F}_I\,\boldsymbol{dt}$ is defined as the external impulse at the contact point. From Eq. (5), the velocity increment of the joint variables is obtained as

$$\Delta\dot{\boldsymbol{\phi}}_a = [\boldsymbol{I}^*_{aa}]^{-1}[\boldsymbol{G}_a^{\upsilon_I}]^T\tilde{\boldsymbol{F}}_I \quad (6)$$

and the velocity increment at the contact point is obtained by the following kinematic relationship.

$$\Delta\boldsymbol{\upsilon}_I = [\boldsymbol{G}_a^{\upsilon_I}]\Delta\dot{\boldsymbol{\phi}}_a = [\boldsymbol{G}_a^{\upsilon_I}][\boldsymbol{I}^*_{aa}]^{-1}[\boldsymbol{G}_a^{\upsilon_I}]^T\tilde{\boldsymbol{F}}_I. \quad (7)$$

A. Effective Mass

Now, let us consider a sawing task. A sawing task can be considered as a continuous collision between the teeth of the saw and the chip to be fabricated, and the impulsive force due to collision creates fracture of the chip. We assume that the fracture happens due to the shearing force formed at the bottom of the chip. That is, the lower part of a chip is fractured by the pushing of a tooth.

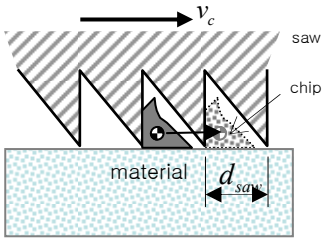

(a) Geometry of saw and chip

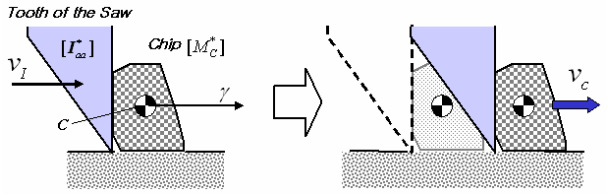

(b) Chip model

Figure 2. Microscopic View of Sawing Task

Based on this condition, a concept of effective mass $[\boldsymbol{M}^*_C]$ is introduced to explain the chip dynamics. Fig. 2 represents the microscopic view of a sawing task. The dynamics of the chip can be described as

$$\tilde{F}_I = [\boldsymbol{M}^*_C]\Delta\upsilon_c/\Delta t_c, \quad (8)$$

where $\tilde{F}_I$ denotes the impulsive force exerted on a chip by the tooth, $\Delta\upsilon_c$ the velocity increment of the chip, Δt_c a period to saw off a piece of chip from the material, respectively. Δt_c can be computed by consideration of the geometry of saw and the sawing velocity

$$\Delta t_c = d_{saw}/\Delta\upsilon_c, \quad (9)$$

where d_{saw} is the distance between two adjacent teeth of the saw, and it is given as $1mm$ in the saw being employed. Now, the effective mass of the chip being sawn is calculated from Eq. (8). Similar to Eq. (6), the velocity increment of the joint variable of the chip is

$$\Delta\boldsymbol{\upsilon}_C = \Delta\dot{\gamma} = [\boldsymbol{M}^*_C]^{-1}(-\tilde{\boldsymbol{F}}_I). \quad (10)$$

B. External Impulse Model of Sawing Task

Assuming that the robot impacts on a surface, substitution of Eq. (7) and Eq. (10) into Eq. (1) gives

$$\left\{\left([\boldsymbol{G}_a^{\upsilon_I}][\boldsymbol{I}^*_{aa}]^{-1}[\boldsymbol{G}_a^{\upsilon_I}]^T + [\boldsymbol{M}^*_C]^{-1}\right)\tilde{\boldsymbol{F}}_I\right\}^T\boldsymbol{n} = -(1+\boldsymbol{e})\left(\boldsymbol{\upsilon}_I - \boldsymbol{\upsilon}_C\right)^T\boldsymbol{n} \quad (11)$$

Then, from Eq. (11), the external impulse can be evaluated as follows:

$$\tilde{\boldsymbol{F}}_I = \left(\frac{-(1+\boldsymbol{e})(\boldsymbol{\upsilon}_I - \boldsymbol{\upsilon}_C)^T\boldsymbol{n}}{\boldsymbol{n}^T\{[\boldsymbol{G}_a^{\upsilon_I}][\boldsymbol{I}^*_{aa}]^{-1}[\boldsymbol{G}_a^{\upsilon_I}]^T + [\boldsymbol{M}^*_C]^{-1}\}\boldsymbol{n}}\right)\boldsymbol{n}, \quad (12)$$

where $[\boldsymbol{I}^*_{aa}]$ denotes the inertia matrix of the robot grasping a saw and $[\boldsymbol{G}_a^{\upsilon_I}]$ represents the Jacobian of the contact point referenced to the joint input variables of the robot. It is noted that the external impulse is the function of robot configuration and the dynamic parameters of the sawing task. The value of $\boldsymbol{e}$ is 0 for purely plastic collisions (the colliding bodies have zero relative velocity to each other at the point of contact immediately after collision) and 1 for purely elastic collisions. Values of $\boldsymbol{e}$ between 0 to 1 indicate intermediate cases of the above two.

For the situation of a robot arm in contact with a solid object, such as a wall, we have the condition, $\upsilon_C = \Delta\upsilon_C = 0$. And the contact impulse force $\tilde{\boldsymbol{F}}_I$ is derived as

$$\tilde{\boldsymbol{F}}_I = \left(\frac{-(1+\boldsymbol{e})(\boldsymbol{\upsilon}_I)^T\boldsymbol{n}}{\boldsymbol{n}^T\left([\boldsymbol{G}_a^{\upsilon_I}][\boldsymbol{I}^*_{aa}]^{-1}[\boldsymbol{G}_a^{\upsilon_I}]^T\right)\boldsymbol{n}}\right)\boldsymbol{n}. \quad (13)$$

For the sawing task, the object to be sawn is initially stationary and the sawn chip deforms permanently. Thus,

we have $\upsilon_c = 0$ and $e = 0$. The external impulse force F_I for the sawing task is then given by

$$\tilde{F}_I = \left(\frac{-(\upsilon_I)^T n}{n^T \{[G_a^{\upsilon_I}][I_{aa}^*]^{-1}[G_a^{\upsilon_I}]^T + [M_C^*]^{-1}\} n} \right) n , \quad (14)$$

where the first term and the second term of the denominator represents the effective dynamics contributing to the external impulse force. The first term is associated with the manipulator dynamics. Meanwhile, the second term is associated with the material property of the chip to be sawn. Thus, the hardness of the object to be sawn changes the magnitude of the external impulsive force. Bigger impulsive force would be required to saw out rather hard material as compared to soft material. The second term explains this phenomenon.

III. Impulse Geometry and Measure

Many former researchers have developed various impulse geometries and impulse measures to evaluate the ability to withstand external impulse. In this chapter, we introduce various external impulse measures and impulse geometries.

Walker[1] proposed *external (dynamic) impulse ellipsoid* that represents relative magnitudes of the external impulsive forces corresponding to the unit ball of changes in joint velocities of the robot. Based on Eq. (6), the dynamic impulse ellipsoid in $\Re^m$ is described as

$$(\tilde{F}_I \in \Re^m : \tilde{F}_I^T [G_\phi^{\upsilon_I}][I_{\phi\phi}^*]^{-2}[G_\phi^{\upsilon_I}]^T \tilde{F}_I \le 1) . \quad (15)$$

From Eq. (6), the dynamic impulse ellipsoid is formed by those contact impulse forces $\tilde{F}_I$ that correspond to changes in joint velocities $\Delta\dot{\phi}$ with unit norm or less, i.e., $\left\|\Delta\dot{\phi}\right\|^2 = \Delta\dot{\phi}^T \Delta\dot{\phi} \le 1$.

However, this method does not consider the magnitude and direction of the velocity, which plays an important role in the magnitude of the external impulse. And also the magnitude of this ellipsoid does not directly represent the impact force.

Kim, et al.[6] proposed a *normalized impact geometry* for serial manipulators. Consider Fig. 3 in which let n be the unit normal vector to the environment and v_I is the pre-impulse velocity to the normal direction of the object to be fabricated. *Normalized impulse geometry* in $\Re^m$ based on $n^T v_I$ is defined by

$$\left| n^T \upsilon_I \right| \le 1 . \quad (16)$$

Then,

$$n^T ([G_\phi^{\upsilon_I}][I_{\phi\phi}^*]^{-1}[G_\phi^{\upsilon_I}]^T) n \frac{F_{imp}}{1+e} \le 1. \ (n \in \Re^m) \quad (17)$$

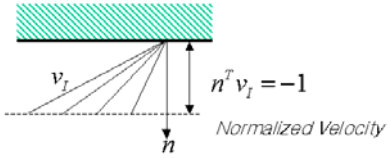

Figure 3. Normalized task velocity

This means the range of directional impact force for given n-directional task velocity like Eq. (16). The magnitude and direction of task velocity, which play an important role in the magnitude of impulsive force, are considered in this geometry.

The normalized impact geometry can be extended to parallel manipulators like dual-arm. It is defined by

$$n^T ([G_a^{\upsilon_I}][I_{aa}^*]^{-1}[G_a^{\upsilon_I}]^T) n \frac{F_{imp}}{1+e} \le 1, \ (n \in \Re^m) \quad (18)$$

where, $[I_{aa}^*]$ represent the inertia matrix referenced to the independent joint set, and $[G_a^{\upsilon_I}] \in \Re^{3 \times N_a}$ is the 1st order KIC relating the contact point's velocity υ_I to the independent joint's velocity, respectively.

The normalized impact geometry is obtained from Eq. (18) by calculating the maximum value of F_{imp} for each direction of n. The resulting ellipsoid is a form of belted ellipsoid.

From Eq. (12), we define the external impulse measure. In case of the sawing task, the velocity vector of the saw has the same direction as n. That is, $\upsilon_I = |\upsilon_I| n$ (refer to Fig. 2). Also note that e becomes zero in the manufacturing tasks yielding plastic deformation of the part to be fabricated. Thus, the external impulse measure for the sawing task is defined as

$$F_{imp} = \frac{-|\upsilon_I|}{n^T \{[G_a^{\upsilon_I}][I_{aa}^*]^{-1}[G_a^{\upsilon_I}]^T + [M_C^*]^{-1}\} n} , \quad (19)$$

where F_{imp} is the magnitude of normalized external impulse.

IV. Simulation and Experiments

A. Simulation

Human sawing task is modeled with the parameters of male adults [5]. The numerical values of the kinematic and dynamic parameters used in simulation are presented in Table 1. Fig. 4 (a) and Fig. 4 (b) represent models of human sawing tasks using single arm and dual-arm, respectively. Human sawing task using a single arm is modeled as a 3 link planar serial manipulator. And human sawing task using a dual-arm is modeled as a 6 joints planar manipulator. θ_1 (θ_4), θ_2 (θ_5), and θ_3 (θ_6) represent the shoulder joint, elbow joint, and wrist joint of the human arm, respectively. And the third link represents the human hand grasping the sawing tool. The purpose of sawing task will be to maximize the external impulse exerted on the object to be sawn by the saw.

TABLE I. Kinematic/Dynamic Parmeters of Human Model

	Length(m)	Mass(kg)	Inertia(Izz ; $kg \cdot m^2$)
l_1	0.33	2.10	0.0208
l_2	0.26	1.274	0.00786
l_3	0.5	0.80	0.0355
l_4	0.33	2.10	0.0208
l_5	0.26	1.274	0.00786
l_b	1.0	-	-

We investigate the distribution of external impulse for the given model. It is assumed that the velocity of the moving saw is 0.1 m/s to the right direction. Coefficient of restitution e is assumed zero because of the plastic

deformation of the object being sawn. Test workspace is a rectangular region given by $0.35 \le x \le 0.65$ (m) and $-0.4 \le y \le 0.4$ (m), as displayed in Fig. 4. We divide the workspace into upper workspace (y>0) and lower workspace (y<0) in simulation.

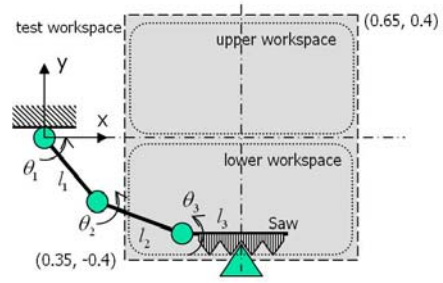

(a) Single Arm Model

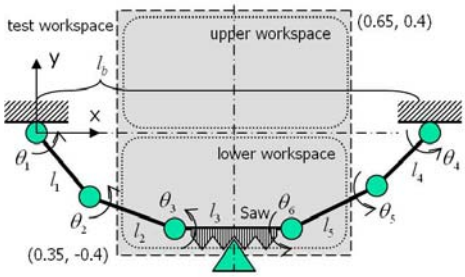

(b) Dual-Arm Model

Figure 4. Models of Human Sawing Task

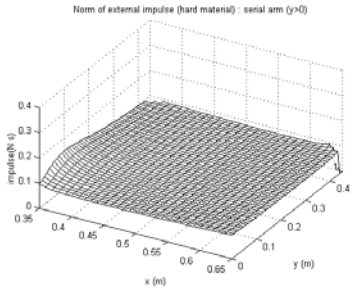

(a) Upper Region(hard material case)

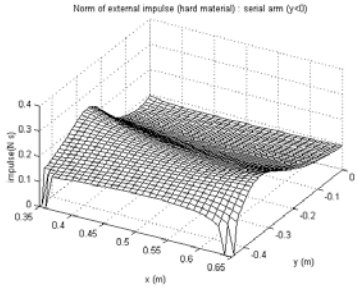

(b) Lower Region(hard material case)

Figure 5. Distribution of External Impulse using Single Arm

The external impulse distributions of the single and dual arm systems are depicted in Fig. 5 through Fig. 6. Here, Fig. 5 is for the case of sawing task by using a single arm, Fig. 6 is for the case of sawing task by using a dual-arm, respectively. The height of the plots denotes the amount of the external impulse evaluated at each position.

The result of the analysis is as follows ;

(a) The lower workspace has better performance in aspect of external impulse ; compare Fig. 5(a) to Fig. 5(b). Thus, the posture of the worker and the workspace of the sawing task are important factors to maximize the external impulse.

(b) Dual-arm can generate larger external impulse than single arm ; compare Fig. 5(b) to Fig. 6(a).

The external impulse for sawing soft materials is less than that for sawing a relatively hard material ; compare Fig. 6(a) to Fig. 6(b).

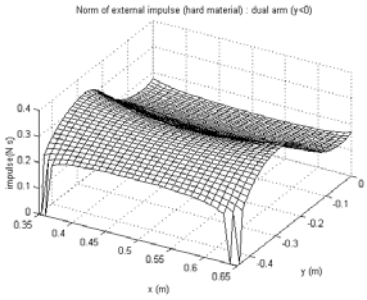

(a) hard material(Lower Region)

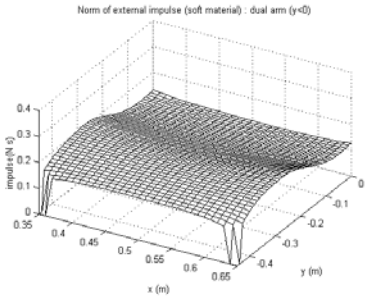

(b) soft material(Lower Region)

Figure 6. Distribution of External Impulse by using Dual-Arm

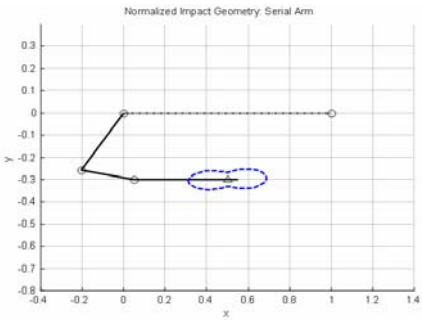

(a) Optimal Region (x, y)=(0.3, -0.3)

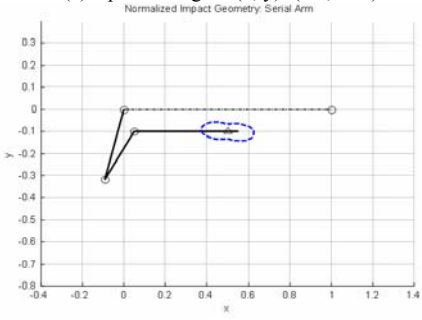

(b) Non-optimal Region (x, y)=(0.3, -0.1)

Figure 7. Normalized External Impulse Geometry

The characteristics of the external impulse can be also observed in terms of the impulse geometry. Fig. 7 denotes the impulse geometry described by the normalized impact geometry given in Eq. (17). The dashed line denotes the external impulse. It is observed that the external ellipsoid for the optimal region is larger than that of the non-optimal region; compare Fig. 7 (a) and (b).

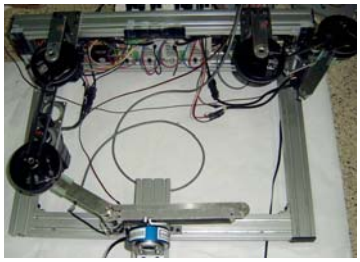

(a) Single Arm Test-bed

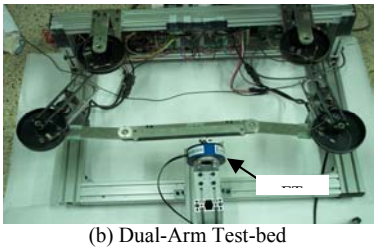

(b) Dual-Arm Test-bed

Figure 8. Figure of Test-bed for Sawing Task

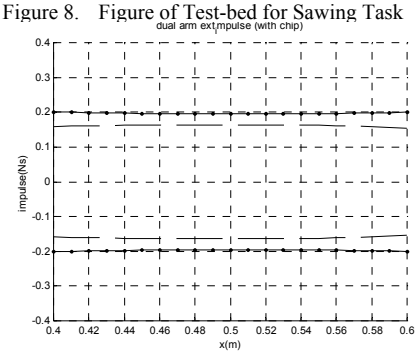

(dashed : non-optimal region, solid : optimal region)

(a) Simulation Result

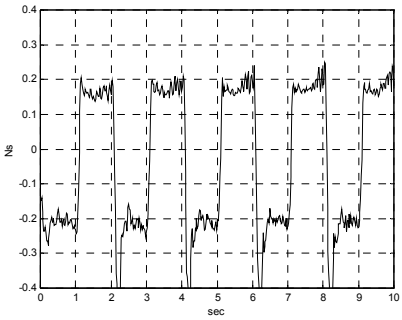

(b) Optimal Region (experimental result)

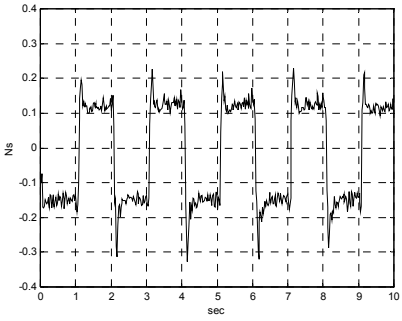

(c) Non-optimal Region (experimental result)

Figure 9. External Impulse Profile of Dual-Arm Sawing Task with Soft Material

According to the results of the above analysis, an optimal sawing region can be identified in which the amount of external impulse is maximized. The workspace along the x direction with the value of y around -0.3m is found the optimal sawing region. This result is coincident to the human experience.

B. Experiments

Fig. 8 (a) and (b) represent 3 DOF planar single and dual arm systems, respectively, for sawing task. Direct Drive AC motors, control hardware, and wire transmission mechanism are employed in this system. This test-bed is designed with the human parameters of Table 1. To measure the sawing force acting on the material, we employ a FT sensor and the material to be sawn is fixed in a gripper mounted on the force sensor. Continuous impulse values are computed from the force data measured by the force sensor. Single and dual arms' sawing tasks to saw off soft and hard materials are performed. Plastic and steel slices are used as soft and hard materials, respectively. Each sawing task is executed at optimal($y = -0.30$) and non-optimal($y = -0.45$) region and performances of these tasks are compared. All sawing tasks are performed with velocity of $0.1m/s$ and a sawing period of 2 sec.

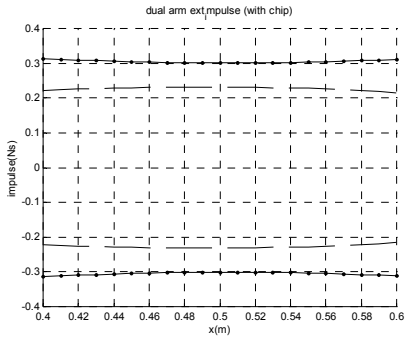

(dashed line : non-optimal region, solid line : optimal region)

(a) Simulation Result

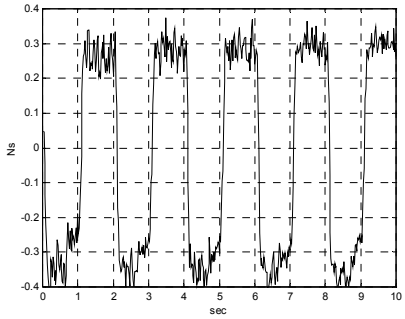

(b) Optimal Region (experimental result)

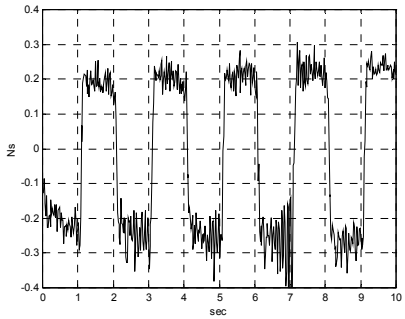

(c) Non-optimal Region (experimental result)

Figure 10. External Impulse Profile of Dual-Arm Sawing Task with Hard Material

Fig. 9 (a) represents the simulation result of the external impulse for the sawing task using a dual-arm with soft material whose effective mass is calculated as 3.2kg by Eq. 8. In this simulation result shown in Fig. 8(a), the solid line denotes the impulse profile for the optimal region and the dashed line denotes the impulse profile for the non-optimal region. Fig. 9(b) and (c) show experimental impulse profiles for optimal and non-optimal region, respectively. The external impulse was calculated by measuring the force data and numerical integration of it for interval of 10ms. It is observed from these graphs that the impulse value at the optimal region is larger than that of the non-optimal region. And the simulation result accords well with the experimental result. Thus, this illustrates that the model for the effective mass is valuable.

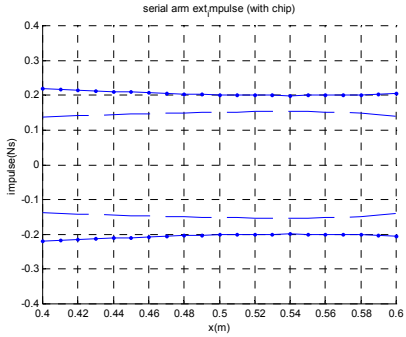

(dashed line : non-optimal region, solid line : optimal region)
(a) Simulation Result

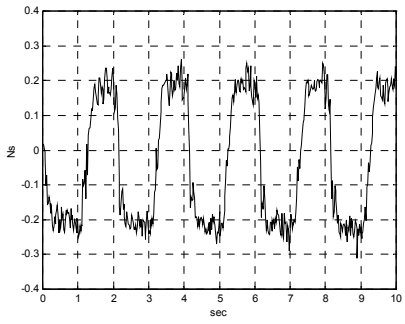

(b) Optimal Region (experimental result)

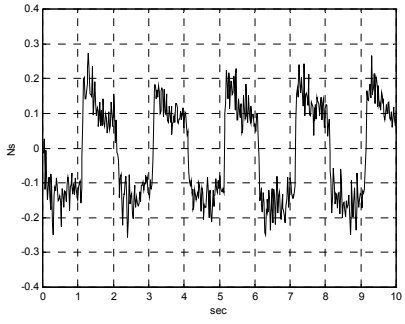

(c) Non-optimal Region (experimental result)
Figure 11. External Impulse Profile of Single Arm Sawing Task with Hard Material

Fig. 10 represents the simulation and experimental results for dual-arm sawing task with hard material whose effective mass is calculated as about 7.5kg. Like Fig. 9, large external impulses are achieved at the optimal region. And the overall magnitude of the external impulse for a hard material is larger than that for soft material. Fig. 11 represents the simulation and experimental results for a single arm sawing task with hard material whose effective mass is about 7.5kg. Like dual-arm sawing task, large external impulses are achieved at the optimal region. It is observed that the overall magnitude of the external impulse for dual-arm sawing task is larger than that for a single arm sawing task. This illustrates another merit of using a dual-arm, compared to a single arm.

V. CONCLUSION

In the robotic manufacturing tasks such as sawing works, the amount of external impulse exerted on the object is an important control parameter. In this paper, a new concept of effective mass is introduced to model the impact phenomenon in the sawing task. Using this concept, the external impulse model of sawing tasks is suggested. Several simulations and experiments are performed for single and dual arms. Both soft and hard work-pieces are tested to justify the external impulse model in the sawing task. The feasibility of the proposed external impulse model is demonstrated by experimental work. Another merit of using the dual-arm is also shown in the view point of external impulse, through the sawing task.

General conclusion is that the external impulse exerted on objects and joints largely depends on the geometry and dynamic characteristics of manufacturing tasks. Specifically, utilization of dual-arms or multiple arms is effective to enhance the performance of the sawing task in aspect of maximizing external impulse and minimizing internal impulse of the joints.

ACKNOWLEDGMENT

This work is partially supported by the Korea Health 21 R&D Project, Ministry of Health and Welfare, Republic of Korea, under Grant 02-PJ3-PG6-EV04-0003.

REFERENCES

[1] I.D. Walker, "Impact configurations and measures for kinematically redundant and multiple armed robot systems", *IEEE Transactions on Robotics and Automation*, Vol. 10, No. 5, pp. 670-683, 1994.

[2] H.-T. Liao and M.C. Leu, "Analysis of impact in robotic peg-in-hole assembly", *Robotica*, Vol. 16, No. 3, pp. 347-356, 1998.

[3] Y.-F. Zheng and H. Hemami, "Mathematical modeling of a robot collision with its environment", *Journal of Robotic Systems*, Vol. 2, No. 3, pp. 289-307, 1985.

[4] J. Wittenburg, *Dynamics of systems of rigid bodies*, B.G. Teubner, Stuttgart, 1977.

[5] D.B. Chaffin, B.J. Gunnar, and Anderson, "Occupational Biomechanics", A Willey-Interscience Publication, John wiley & sons, 1984.

[6] J. Kim, W.K. Chung, and Y. Youm, "Normalized Impact Geometry and Performance Index for Redundant Manipulators," proceedings of the 2000 IEEE International Conference on Robotics and Automation, pp. 1714-1719, 2000.

[7] S.H. Lee, B.-J. Yi, S.H. Kim, and Y.K. Kwak, "Modeling and Analysis of Internal Impact for General Classes of Robotic Mechanism", Proceeding of IEEE /RSJ International Conference on Robotics and Systems, pp. 1955-1962, 2000.

[8] G. Ferretti, G. Magnani, and A. Zavala Rio, "Impact modeling and control for industrial manipulators", IEEE Control System Magazine, Vol. 18, No. 4, pp. 65-71, 1998.

[9] J.H. Lee, B.-J. Yi, S.R. Oh, Il Hong Suh, "Impulse Measure Based Performance Analysis of Sawing Task by Dual Arm," Proceeding of IEEE International Conference on Robotics and Automation, pp. 982-988, 2002.